ORIGINAL RESEARCH

Design and Driving Performance Study of Soft Actuators for Hand Rehabilitation Training

Zhilin Zhang [ID][1–4], Aldrin D Calderon[2], Xingyu Huang[5], Guixian Wu [ID][6], Chuanjian Liang [ID][1,3,4]

[1]School of Physics and Telecommunications Engineering, Yulin Normal University, Yulin, People's Republic of China; [2]School of Mechanical, Manufacturing and Energy Engineering, Mapua University, Manila, Philippines; [3]Center for Applied Mathematics of Guangxi, Yulin Normal University, Yulin, People's Republic of China; [4]Guangxi Universities Key Laboratory of Complex System Optimization and Big Data Processing, Yulin Normal University, Yulin, People's Republic of China; [5]School of Information Technology, Mapua University, Manila, Philippines; [6]Yulin Health School of Guangxi Medical University, Yulin, People's Republic of China

Correspondence: Chuanjian Liang, Email lcj19@ylu.edu.cn

Purpose: To address the application requirements of soft actuators in rehabilitation training gloves, and in combination with ergonomic requirements, we designed a segmented soft actuator with bending and elongation modules. This actuator can achieve independent or coupled movements of the finger joints.

Methods: A finite element model of the joint actuator was established to compare the driving performance of actuators with different structural forms. Numerical calculations were used to analyze the effects of structural size parameters on the bending characteristics and end output force of the actuator. The design was then refined based on these analyses.

Results: The joint actuator designed in this study demonstrated a 71% increase in bending angle compared to the standard fast pneumatic network structure. Key factors affecting the driving performance include the thickness of the constraint layer, the inner wall thickness of the chamber, chamber height, chamber width, chamber spacing, chamber length, and the number of chambers. After improvements, the bending angle of the joint actuator increased by 60.6%, and the output force increased by 145.9%, indicating significant improvement.

Conclusion: This study designed and improved a soft actuator for hand rehabilitation training, achieving independent and coupled joint movements. The bending angle, bending shape, and joint driving force of the soft actuator meet the requirements for finger rehabilitation training.

Keywords: rehabilitation training, soft actuators, fast pneumatic networks, structural optimization, finite element method

Introduction

As the global population ages rapidly, the incidence of strokes has been increasing annually. The residual limb dysfunctions from strokes, primarily in hand functions, severely impact patients' normal lives. For patients with hand dysfunctions, using rehabilitation training gloves for auxiliary treatment has proven to be an effective method. Traditional rehabilitation training gloves are mostly made of rigid materials,[1,2] which have several drawbacks, including bulkiness, heavy weight, poor fit with fingers, and a risk of causing secondary injuries during use. To address the limitations of rigid structures, researchers have proposed rigid-flexible coupled structures.[3,4] However, these designs only provide a single degree of freedom for the entire flexion and extension of each finger, which cannot meet the complex movement requirements of the human hand. In recent years, with the rapid development of soft robotics technology and new flexible materials, the application research of soft actuators in hand function rehabilitation devices has attracted widespread attention. Soft rehabilitation training gloves rely on soft actuators to provide the driving force, thereby facilitating finger rehabilitation movements. The main driving methods for soft actuators include Pneumatic actuation,[5,6] tendon-actuators,[7] dielectric elastomer,[8] and shape memory alloy[9] actuation, among which pneumatic actuation is widely used due to its simplicity, strong deformation capability, good compliance, and low manufacturing costs.

Common structures of pneumatic soft actuators include pneumatic networks and fiber-reinforced types. Pneumatic networks are further divided into slow pneumatic network structures and fast pneumatic network (fPN) structures.[10] The fast pneumatic network structure is increasingly favored by researchers due to its low required pressure and superior bending characteristics. Polygerinos et al from Harvard University[11] proposed applying the pneumatic network structure to rehabilitation gloves, where finger movement is driven by the different elongation rates of the upper and lower layers during inflation, causing bending. Li et al[12] proposed a dual-chamber soft actuator, which produces a greater output force compared to a single-chamber actuator but has a smaller bending angle. Cappello et al[13] designed a soft rehabilitation glove based on bidirectional fabric soft actuators. These soft actuators can only produce bending with consistent curvature, leading to poor fit with fingers. To address this limitation, Polygerinos et al[14] designed a soft rehabilitation glove with a fiber-reinforced structure, while Li et al[15] proposed a segmented pneumatic actuator with variable stiffness for a soft rehabilitation glove. Wang et al[16] designed a segmented pneumatic soft actuator with embedded airbags based on the characteristics of the human hand structure, improving the fit with fingers, but the embedded airbags increase the complexity of the structure. Additionally, most of these soft actuators are designed as overall bending structures, and the joints cannot bend independently, limiting flexibility. Wang et al[17] designed a segmented pneumatic network bidirectional bending actuator, where each joint is independently driven, improving flexibility. However, this design has a relatively large overall structure, affecting comfort when worn. Liu et al[18] improved the fit with fingers by embedding segmented spring steel strips at the bottom of the soft actuator, but the Introduction of spring steel strips increased the complexity of the structure.

The performance of soft actuators directly impacts the effectiveness of rehabilitation training gloves. To enhance the performance of soft actuators, researchers have conducted extensive studies.[19–22] Hu et al[23] analyzed the effects of design parameters such as the thickness of the underlying layer, chamber gaps, and chamber wall thickness on actuator performance, identifying patterns in how each parameter influences performance. Yang et al[24] introduced the free bottom actuator (FBA), which significantly improved the bending angle and output force of the actuator by removing the constraints at the bottom of the airway sections in the fast air network structure. Lee et al[25] systematically studied how parameters such as chamber shape, number of chambers, and the shape and size of the bottom cross-section affect driving performance. The design of soft actuators used in rehabilitation training gloves must fully consider ergonomic requirements, however, the aforementioned studies did not fully address these requirements.

This paper addresses the application needs of soft actuators in rehabilitation training gloves based on ergonomic requirements, designing a segmented pneumatic soft actuator with bending and elongation modules. The bending module employs a fast pneumatic network structure, while the elongation module utilizes a slow pneumatic network structure. Each joint can be independently controlled, featuring capabilities for independent or coupled motion. The finite element method is used to study the influence of structural parameters on the actuator's driving performance and to optimize these parameters, enhancing the actuator's performance.

Soft Actuator Structural Design
Finger Structure Analysis
The main purpose of hand rehabilitation training devices is for the rehabilitation of stroke patients' hands. Through repeated motion training, patients gradually regain the motor functions of their fingers. To achieve effective training results, the structural design of the training device must meet ergonomic requirements. The primary movement patterns of the human hand include grasping, hooking, pinching, and dynamic manipulation. These movement patterns are achieved through the bending, extension, abduction, and adduction movements of the finger joints, and these movements are closely related to the structural characteristics of the fingers. The finger structure consists of multiple bones; taking the index finger as an example, it includes the distal phalanx(DP), middle phalanx(MP), and proximal phalanx(PP). These bones are connected to a series of joints and ligaments, relying on tendons to flex and extend the joints, as shown in Figure 1. The joints of the index finger include the metacarpophalangeal joint (MCP), the proximal interphalangeal joint (PIP), and the distal interphalangeal joint (DIP). The MCP joint is a biaxial joint that can perform flexion,
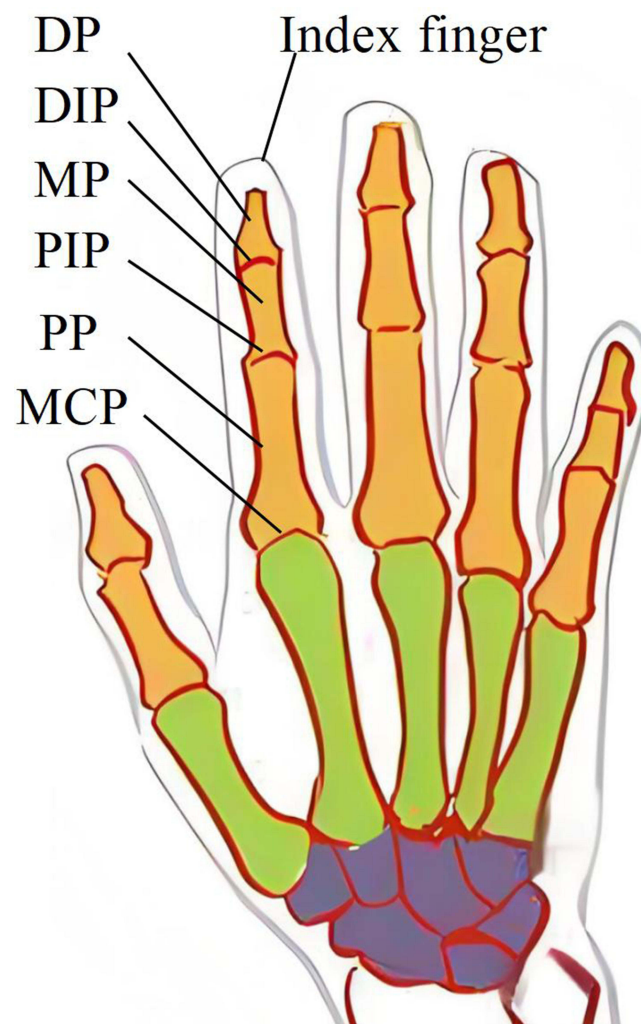
Figure 1 Schematic Diagram of the Index Finger Structure.

abduction, and adduction movements, while the other joints can only perform flexion. The range of motion for each joint is listed in Table 1.[26]

Design of Drive System Structures

The actuator, as the main driving component of hand rehabilitation training devices, has a decisive impact on the effectiveness of the rehabilitation outcomes provided by these devices. Considering the aspects of safety and convenience of use, the rehabilitation training devices employ pneumatic soft actuators as their driving elements. To meet ergonomic requirements, the soft actuators designed in this study adopt a segmented structure, with each joint and phalanx

Table 1 Range of Motion of Each Joint in the Index Finger

Joint	Motion Direction	Range of Motion (degrees)
MCP	Flexion-Extension	−10~90
PIP	Flexion-Extension	0~120
DIP	Flexion-Extension	0~90

independently designed and driven. Given the wide range of bending angles at different finger joints, each joint actuator employs a fast pneumatic network structure, which offers significant advantages in terms of large deformations, high output force, and low strain. The standard fast pneumatic network structure,[10] primarily comprising chambers, a constraining layer, and air channels, is elongated in shape with an internal rectangular thin-wall network structure. Each chamber is independent, linked by the constraining layer into a sealed unit, with air channels located at the bottom of the chamber, as shown in Figure 2. Literature[24] notes that the structure connecting the bottoms of adjacent chambers in the standard fast pneumatic network actuator enhances the structural strength to some extent, which is detrimental to the actuator's bending deformation and force output, as indicated in the region I of Figure 2. Differing from the improvements suggested in the Literature,[24] this paper's modification involves removing some of the material on the outer sides of the air channel area, as illustrated in Figure 3. Considering that the relative positions of joints change during finger bending, which may cause the joint actuator to shift relative to the human joint, the phalanx module is designed as an extendable slow pneumatic network structure.

The future development trend of finger rehabilitation training mechanisms is the ability to perform segmented independent movements and to achieve gas-driven flexibility.[27] Accordingly, this paper designs a soft actuator based on the segmented movements of the human finger, taking the index finger as an example. The index finger has three bending joints (MCP, PIP, DIP) and three phalanges (DP, MP, PP). Each position has been modeled and designed accordingly, with the overall soft actuator modeling shown in Figure 4. This soft actuator structure includes an MCP actuator module, a PIP actuator module, a DIP actuator module, a DP phalanx module, an MP phalanx module, and a PP phalanx module, each actuator module featuring an individual air intake.
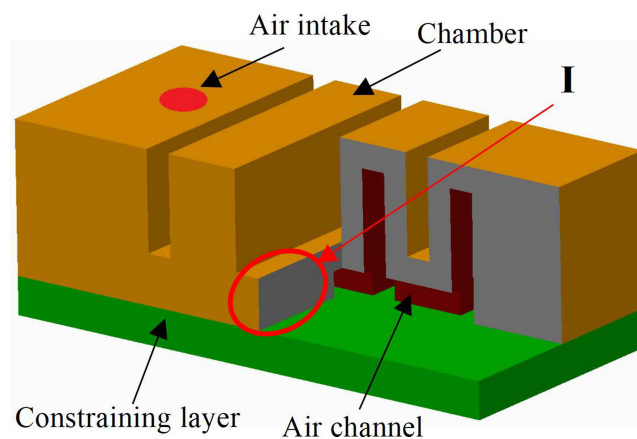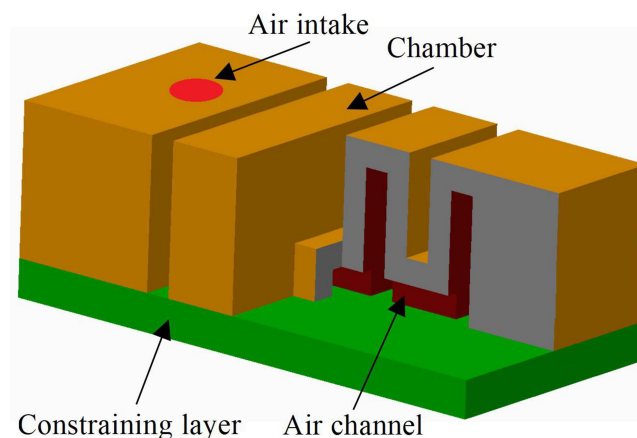

Figure 2 Standard Fast Pneumatic Network Structure.

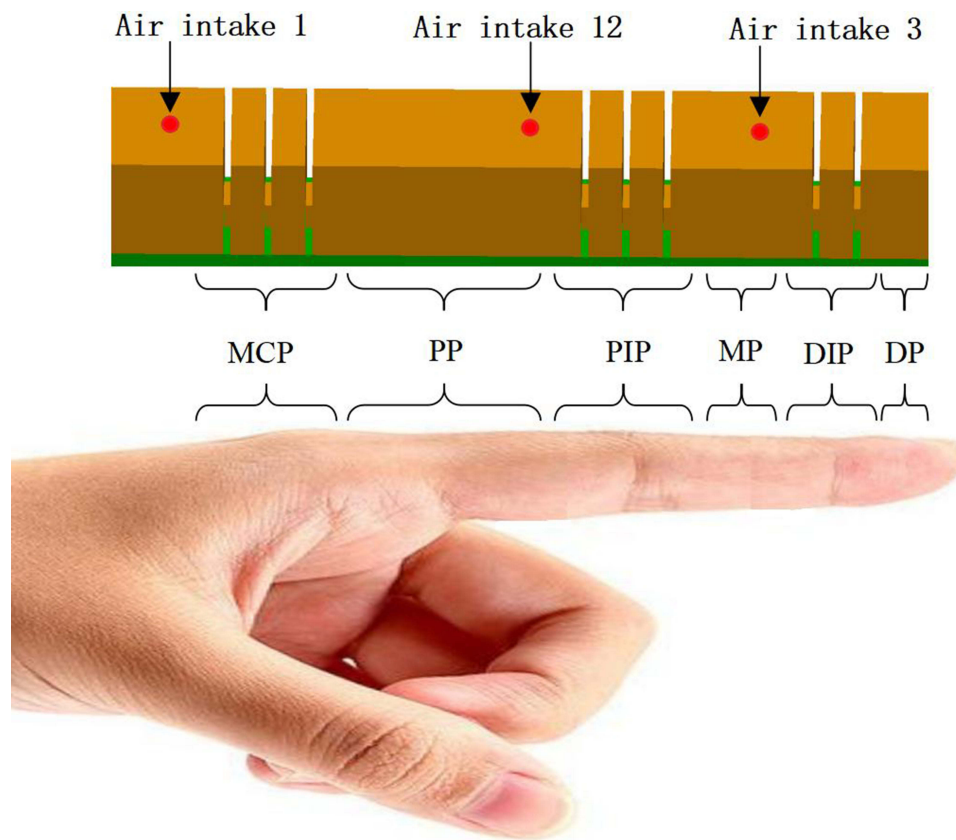**Figure 3** Improved Standard Fast Pneumatic Network Structure.

Figure 4 Schematic Diagram of the Soft Actuator Structure.

The cross-sectional view of the soft actuator model is shown in Figure 5. According to statistical data on the hand dimensions of Chinese males[28] The initial overall dimensions of the structure are a length of 120mm, a height of 15mm, and a width of 20mm. The MCP actuator is located 24mm from the left end, the center-to-center distance between the MCP and PIP actuators is 48mm, and the center-to-center distance between the PIP and DIP actuators is 28mm, with the DIP actuator 20mm from the right end. The left end of the model is fixed. By injecting air pressure into air inlet 1, the MCP actuator can be bent; injecting air into air inlet 2 bends the PIP actuator; and injecting air into air inlet 3 bends the DIP actuator. The higher the injected air pressure, the greater the bending angle. By injecting different pressures into the various air inlets, multiple segmented bending motions of the soft actuator can be achieved. This allows for a variety of bending rehabilitation exercises for the finger.
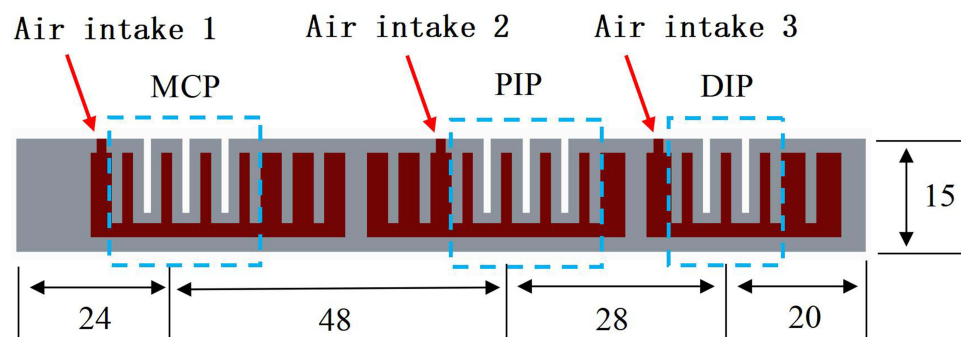
Figure 5 Cross-sectional View of the Soft Actuator.

Finite Element Analysis of Joint Actuators

The joint actuator is the core component of the entire soft actuator system. Conducting finite element analysis on it enables the understanding of its driving characteristics, providing a reference for the improvement and design of soft actuators.

Finite Element Modeling

To analyze the deformation behavior of the joint actuator, a three-dimensional model was constructed in CAXA software. The dimensions of the original model are shown in Figure 6: t1=3mm, t2=2mm, t3=2mm, t4=2mm, t5=2mm, t6=2mm, h=10mm, b=16mm, d=2mm, L1=6mm. The model was then imported into finite element software for finite element modeling. The soft actuator is made from a hyperelastic silicone material M4601, which exhibits large deformations and nonlinear characteristics when deformed. Therefore, the Yeoh hyperelastic model, which is suitable for describing large deformations of hyperelastic materials, is adopted. According to reference,[11] the material constants for M4601 are C10=0.11 and C20=0.02. The finite element model was simplified as much as possible to closely resemble real-world conditions. The inflation inlet at the top and the phalanx module were disregarded, while the internal channels were
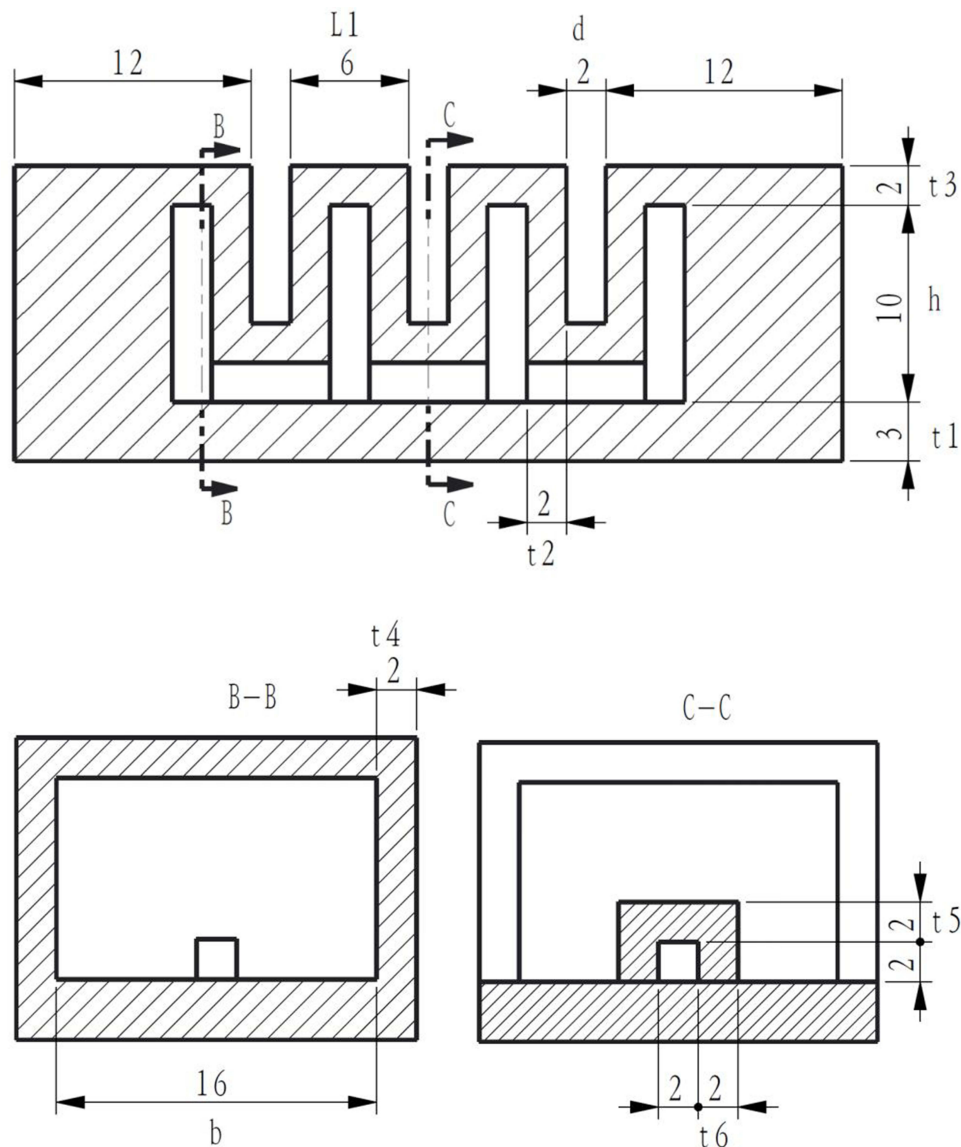
Figure 6 Dimensional Drawing of the Soft Actuator.

retained. To ensure computational accuracy and efficiency, and considering that the actuator is made from an incompressible hyperelastic material, an 8-node hexahedral element was used for meshing the hyperelastic body, with an approximate global seed size of 0.5mm. Figure 7 shows the finite element mesh model of the joint actuator, with a total of 15,074 elements divided.

The loading condition for the model involves applying uniform gas pressure to all internal walls, while the boundary condition consists of a fixed displacement constraint applied to the left end face. A static analysis step is used to analyze the model, considering the large deformations that occur during the operation of the actuator. Geometric nonlinearity is accounted for by activating the geometric nonlinearity switch during the analysis.

Analysis of Numerical Calculation Results

For comparative analysis purposes, calculations were also performed for the fPN structure from Literature[10] and the FBA structure from Literature.[24] The variation in bending angles of soft actuators with different structural forms as a function of input air pressure is shown in Figure 8. When the input air pressure is 50 kPa, the bending displacement contour map is displayed in Figure 9. When calculating the terminal output force of the joint actuator, a displacement constraint in the Y-direction is applied to the nodes at the bottom end of the model (as shown in Figure 10). The terminal output force of
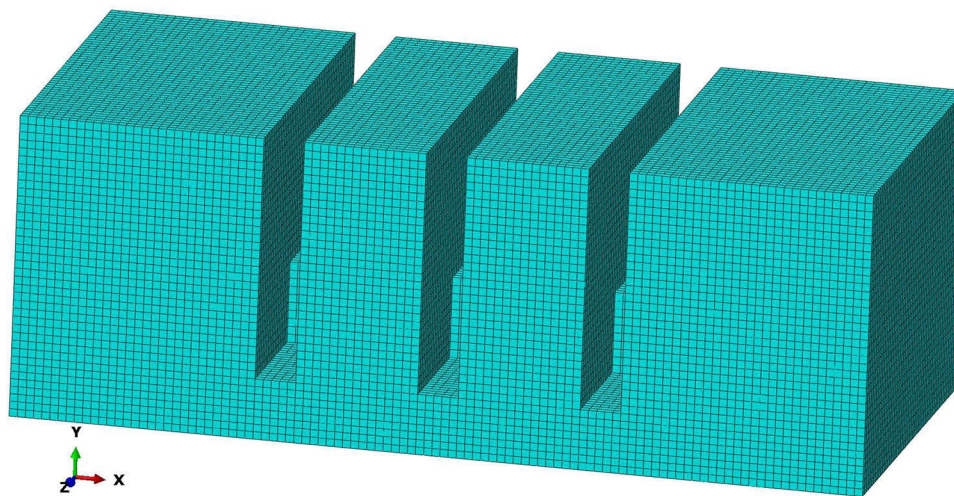

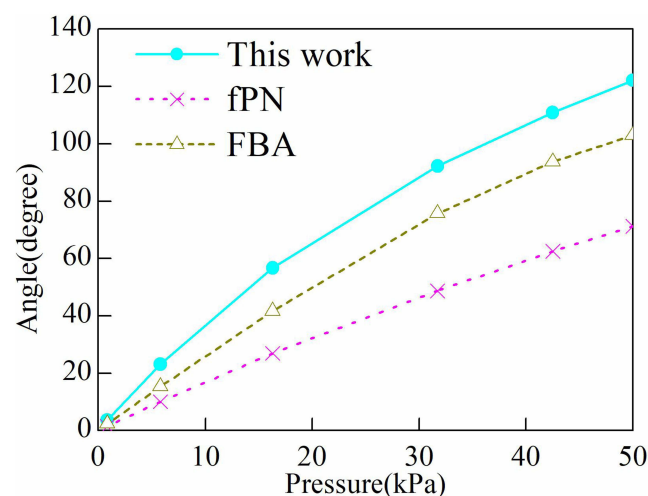**Figure 7** Finite Element Mesh Model of the Soft Actuator.

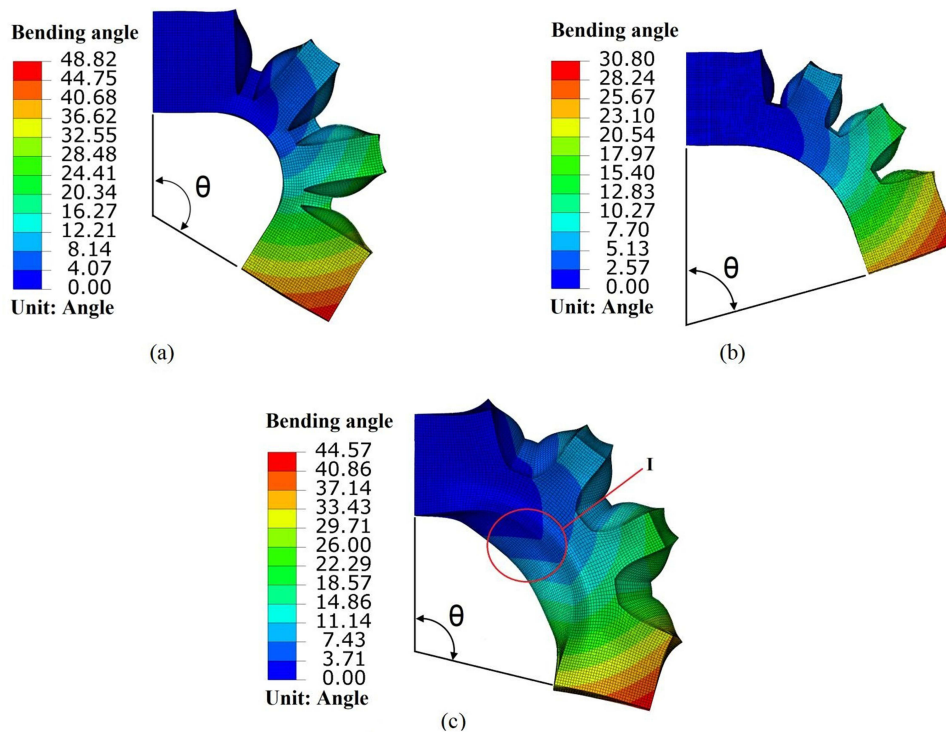**Figure 8** The curve of Bending Angle Variation with Input Air Pressure.

Figure 9 Displacement maps of different structural schemes with an input air pressure of 50kPa. (**a**) shows the displacement diagram of the proposed structure with a bending angle of θ. (**b**) shows the displacement diagram of the fPN structure with a bending angle of θ. (**c**) shows the displacement diagram of the FBA structure with a bending angle of θ.
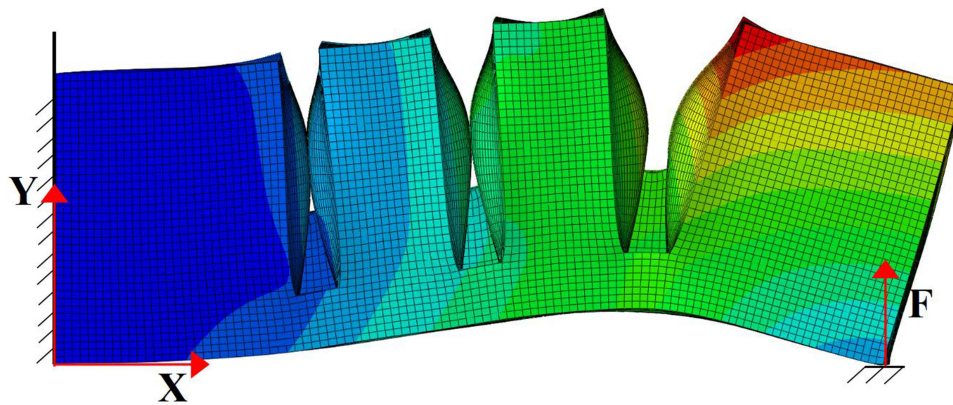

Figure 10 Schematic diagram for calculating end output force.

the actuator can be equivalently represented by the resultant of the reactive forces at these constrained nodes. The variation in terminal output force of soft actuators with different structures as a function of input air pressure is shown in Figure 11.

Figure 8 shows that the bending angles of actuators with different structural forms monotonically increase with increasing input air pressure. Under the same air pressure, the bending angle of the joint actuator described in this paper is greater than those of the other two structural forms. As seen in Figure 9, at an input air pressure of 50 kPa, the bending angle of the soft actuator in this study is 122.13°, compared to 71.25°for the fPN structure and 102.94°for the FBA structure. The bending angle of our actuator is approximately 71% higher than that of the fPN and 19% higher than that of the FBA. (Figure 9c) reveals that during bending, the FBA structure exhibits noticeable bulging at its base (Region I), a phenomenon not observed in the other two structures. This bulging can prevent tight conformity between the actuator
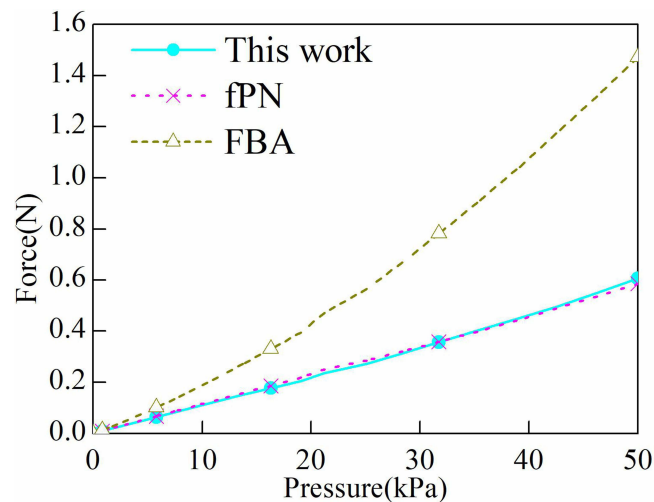
Figure 11 The curve of end output force variation with input air pressure.

base and the human hand, affecting wear comfort. Figure 11 shows that the terminal output forces of actuators with different structures also monotonically increase with increasing input air pressure. Under the same conditions, the terminal output force of the FBA is noticeably higher than that of the other two structures. Considering bending angle as the most critical performance indicator of soft actuators, and taking into account wear comfort, the actuator design presented in this paper is more suitable for use in rehabilitation training devices than the other two designs.

The Impact of Structural Parameters on Drive Performance and Improved Design

The joint actuator utilizing a pneumatic grid structure exhibits bending characteristics that depend not only on the input air pressure but also on the structural parameters themselves. By employing the method of controlling variables, a systematic analysis is conducted on the dimensional parameters that influence the bending angle and end output force of the joint actuator. Based on this analysis, an optimization of the structural parameters is performed. The primary dimensional parameters include the thickness of the bottom constraint layer, the wall thickness of the chambers, the airway wall thickness, the height of the chambers, the width of the chambers, the spacing between chambers, the length of the chambers, and the number of chambers, n.

The Impact of Bottom Constraint Layer Thickness

Calculations were conducted with the thickness of the bottom constraint layer t_1 set at 2 mm, 3 mm, and 4 mm respectively. The results for the bending angle and end output force are shown in Figures 12 and 13 respectively.

Figures 12 and 13 demonstrate that the thickness of the bottom constraint layer significantly affects the performance of the actuator. Under the same air pressure, as the thickness of the constraint layer increases, the bending angle of the actuator tends to decrease, while the end output force shows an increasing trend. The reason for this phenomenon is that an increase in the thickness of the constraint layer enhances the bending stiffness of the actuator, which in turn somewhat limits the bending deformation of the actuator. A too-thin wall thickness may limit the pressure-bearing capacity and result in a smaller end output force. Taking all factors into account, a thickness of $t_1 = 2$ mm was ultimately selected.

The Impact of Chamber Wall Thickness

Chamber wall thickness includes the inner wall thickness of the chamber t_2, the top wall thickness t_3, and the side wall thickness t_4.
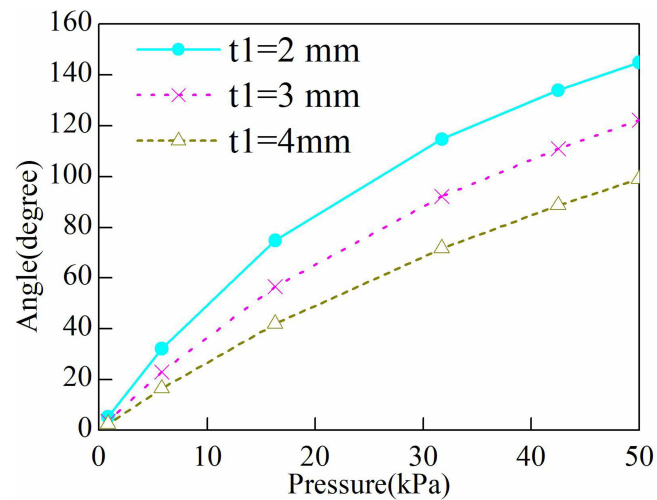
Figure 12 Influence of bottom constraint layer thickness on bending angle.
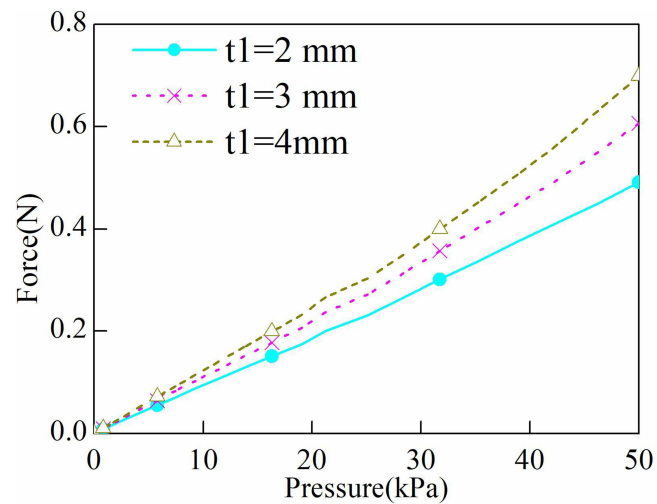

Figure 13 Influence of bottom constraint layer thickness on end output force.

1) Calculations were conducted with the inner wall thickness of the chamber t_2 set at 1.5 mm, 2 mm, and 2.5 mm, respectively. The corresponding results are shown in Figures 14 and 15. The inner wall thickness of the chamber significantly affects both the bending angle and the end output force of the actuator. Under the same air pressure, as the inner wall thickness increases, both the bending angle and the end output force tend to decrease. This is primarily because an increase in the inner wall thickness enhances the chamber's resistance to deformation, effectively increasing the longitudinal tensile stiffness along the upper part of the actuator, thereby reducing both the bending deformation and the end output force. From the perspective of enhancing the bending deformation capability of the actuator, a thinner inner wall thickness is preferable. However, if the thickness is too small, the chamber's pressure-bearing capacity is limited, posing a risk of bursting under high pressures and making manufacturing challenging. Therefore, a thickness of t_2=1.5 mm was ultimately selected.

2) The chamber top wall thickness t_3 was set at 1.5 mm, 2 mm, and 2.5 mm for computational analysis, with corresponding results shown in Figures 16 and 17. The influence of the chamber top wall thickness on the actuator's bending angle and terminal output force is minimal. To prevent excessive radial deformation due to insufficient wall thickness, a final thickness of t_3=2 mm was chosen.
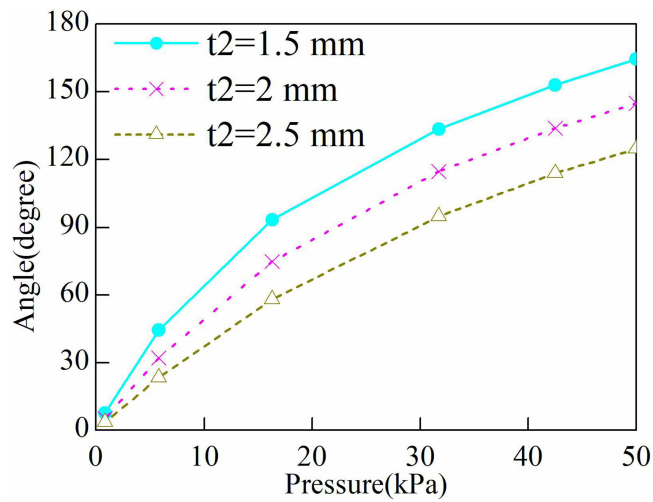
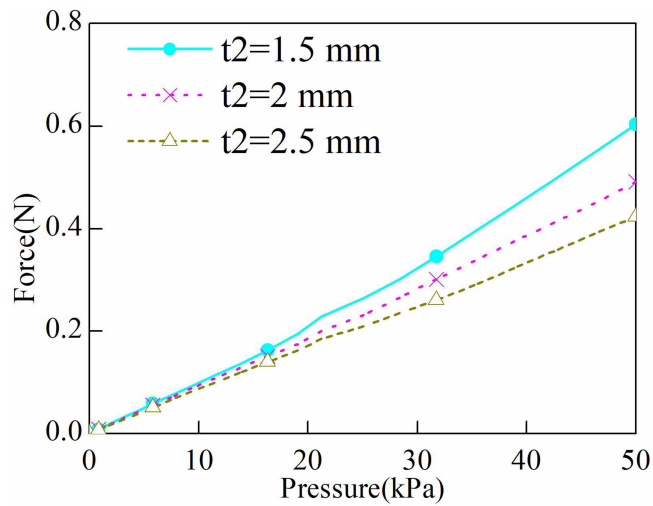**Figure 14** Influence of chamber inner wall thickness on bending angle.

Figure 15 Influence of chamber inner wall thickness on end output force.
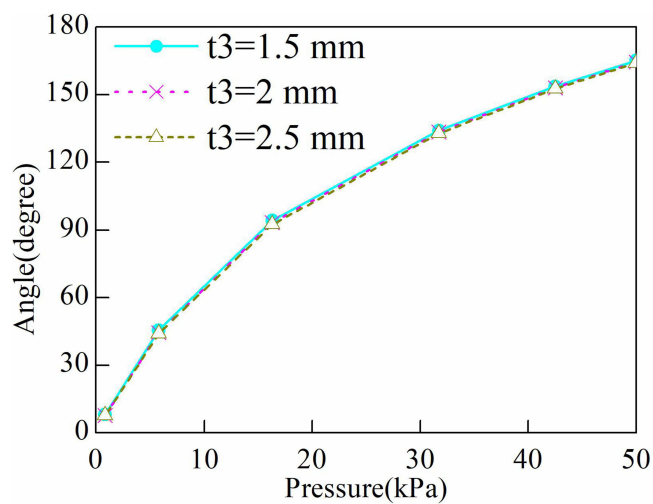

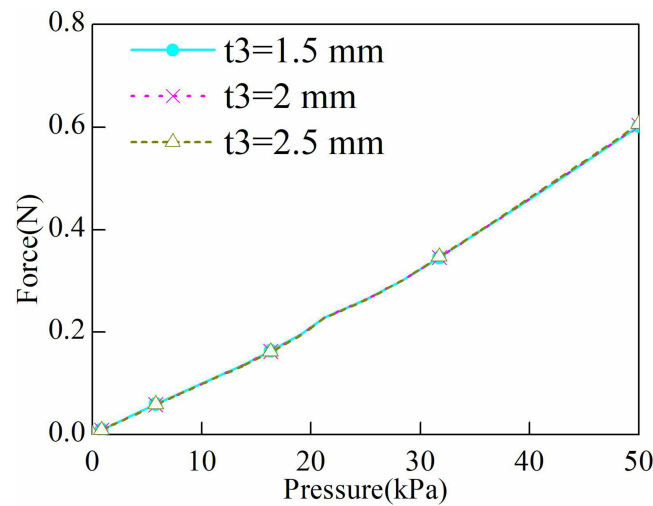**Figure 16** Influence of chamber top wall thickness on bending angle.

Figure 17 Influence of chamber top wall thickness on end output force.

3) The chamber sidewall thickness t4 was evaluated at 1.5 mm, 2 mm, and 2.5 mm through computational analysis, with the results presented in Figures 18 and 19. The impact of the chamber sidewall thickness on the actuator's bending angle and terminal output force was also minimal. To prevent excessive radial deformation resulting from insufficient wall thickness, a final thickness of t4 =2 mm was selected.

The Impact of Airway Wall Thickness
The airway wall thickness includes the airway top wall thickness t5 and the airway side wall thickness t6.

1) The airway top wall thickness t5 was analyzed at 1.5 mm, 2 mm, and 2.5 mm, with the corresponding results shown in Figures 20 and 21. The thickness of the airway top wall has a noticeable impact on the actuator's bending angle and terminal output force. Under consistent air pressure, as the chamber side wall thickness increases, the bending angle of the actuator tends to decrease, while the terminal output force tends to increase. After careful consideration, a final thickness of t5=1.5 mm was chosen.
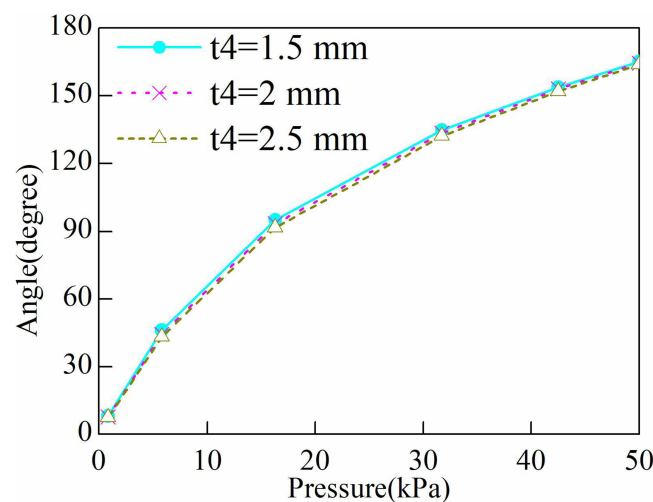

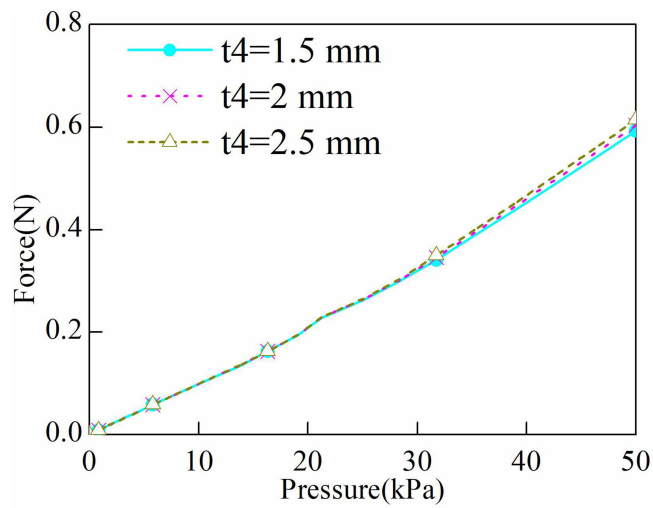**Figure 18** Influence of chamber side wall thickness on bending angle.

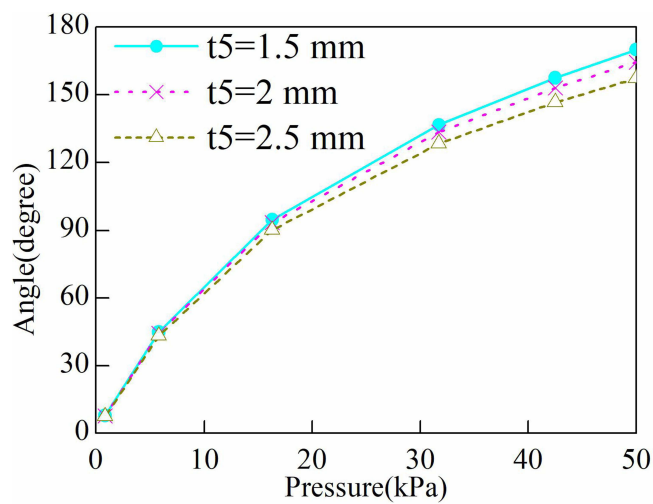**Figure 19** Influence of chamber side wall thickness on end output force.

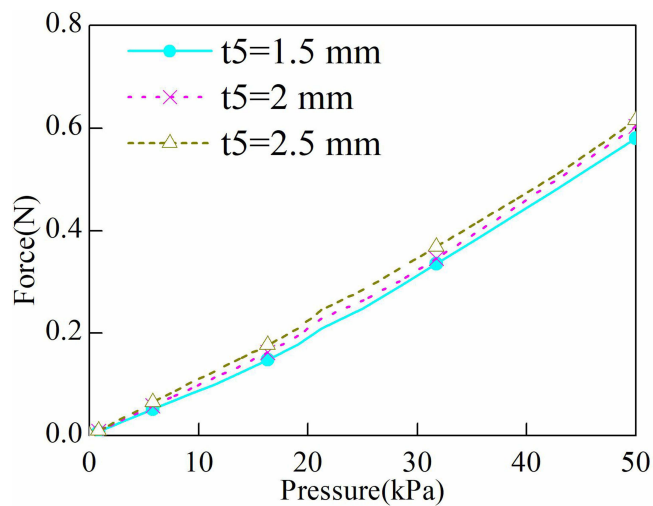**Figure 20** Influence of airway top wall thickness on bending angle.

Figure 21 Influence of airway top wall thickness on end output force.

2) The airway side wall thickness t6 was evaluated at 1.5 mm, 2 mm, and 2.5 mm, with the results presented in Figures 22 and 23. The impact of the airway side wall thickness on the actuator's bending angle and terminal output force was found to be minimal. For ease of manufacturing, a final thickness of t6=2mm was selected.

The Influence of Chamber Height

The chamber height h was set at 8 mm, 10 mm, and 12 mm for computational analysis, with the results for bending angle and terminal output force shown in Figures 24 and 25, respectively. The figures indicate that chamber height has a significant impact on the performance of the actuator. Under the same air pressure, as the chamber height increases, both the bending angle and the terminal output force of the actuator show an increasing trend. This is because a larger chamber height increases the surface area affected by the air pressure, thus enhancing the axial force, which in turn increases both the bending angle and the terminal output force. However, an increase in chamber height also leads to larger dimensions and weight of the actuator, which may reduce the wearable comfort level. Considering all factors, a chamber height of h= 12 mm was ultimately chosen.

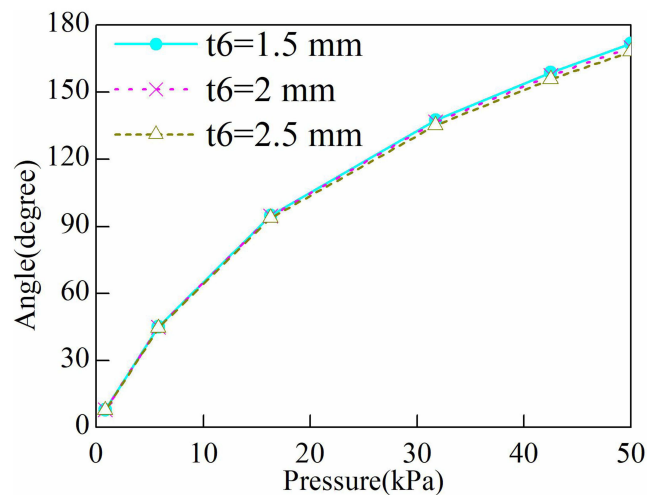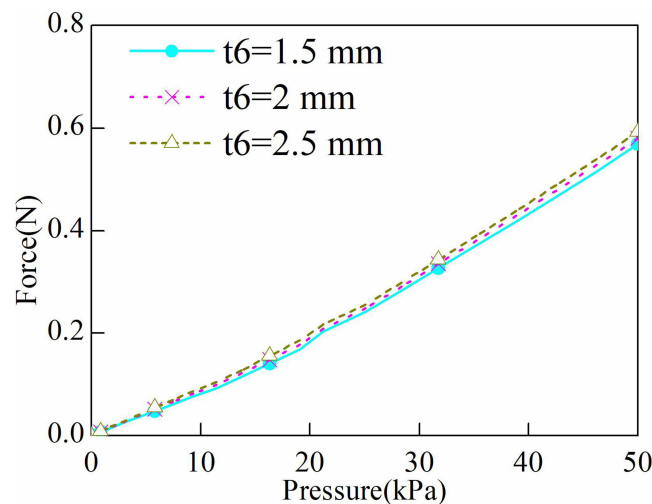**Figure 22** Influence of airway side wall thickness on bending angle.

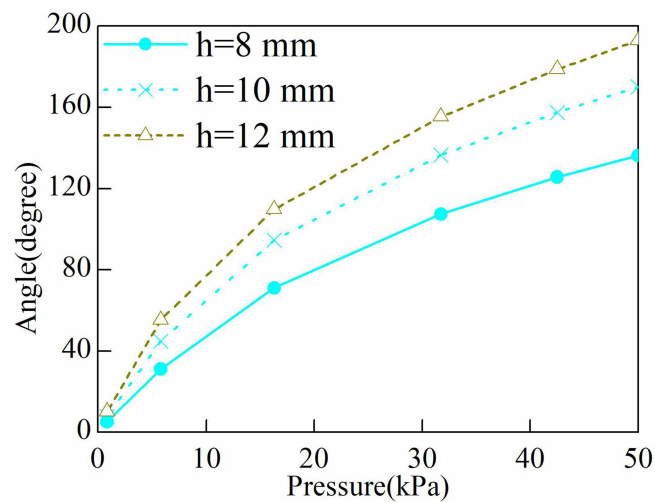**Figure 23** Influence of airway side wall thickness on end output force.

250

Medical Devices: Evidence and Research 2024:17

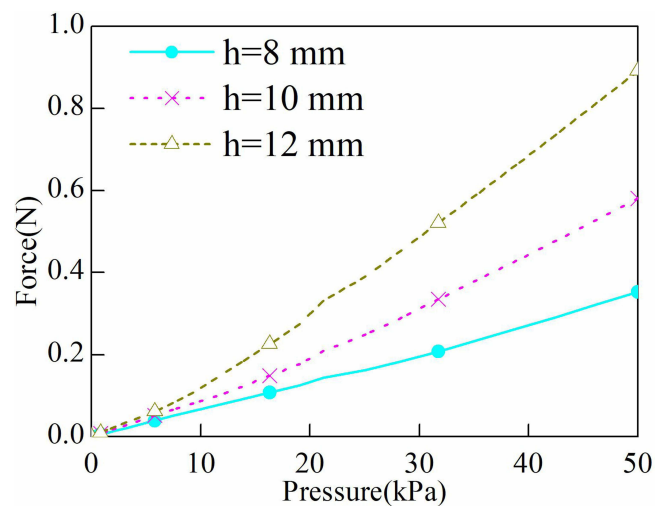**Figure 24** Influence of chamber height on bending angle.

Figure 25 Influence of chamber height on end output force.

The Impact of Chamber Width

Chamber width b was varied at 14 mm, 16 mm, and 18 mm for computational analysis, with the results for bending angle and terminal output force presented in Figures 26 and 27, respectively. The figures indicate that chamber width significantly affects the performance of the actuator. Under the same air pressure, as chamber width increases, both the bending angle and the terminal output force of the actuator exhibit an upward trend. An increase in chamber width enlarges the surface area affected by air pressure, thereby enhancing the axial force, which in turn increases both the bending angle and the terminal output force. However, excessively large chamber widths can also compromise the wearable comfort level. After careful consideration of these factors, a chamber width of b= 16 mm was ultimately selected.

The Impact of Chamber Spacing

Chamber spacing d was varied at 1 mm, 2 mm, and 3 mm for computational analysis, with the results for bending angle and terminal output force presented in Figures 28 and 29 respectively. The data reveal that while chamber spacing has a minor effect on the bending angle of the actuator, it significantly influences the terminal output force. Under constant
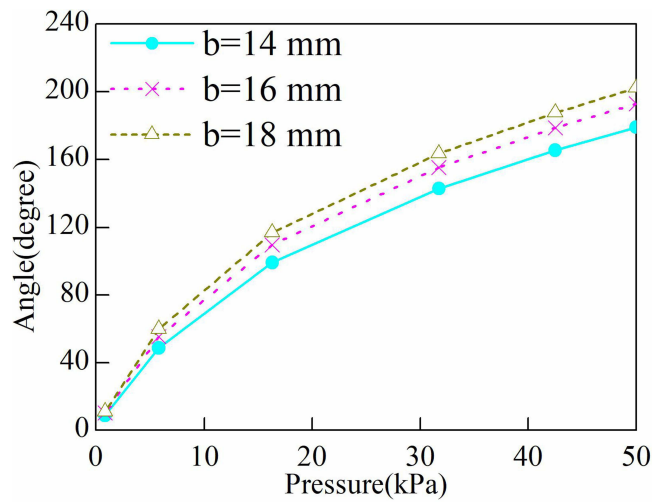
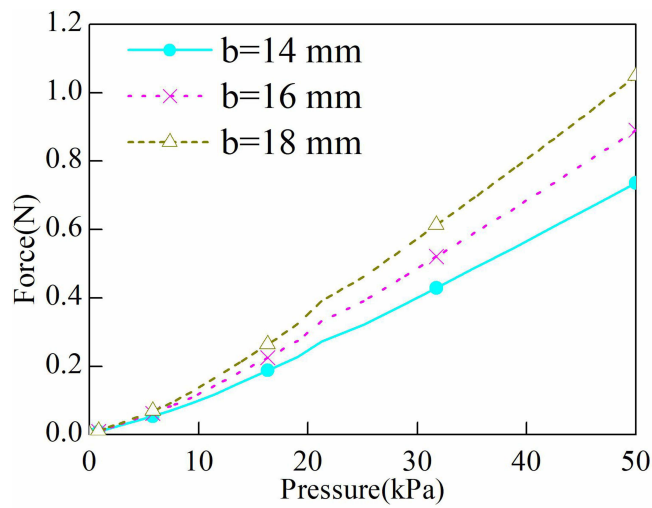**Figure 26** Influence of chamber width on bending angle.

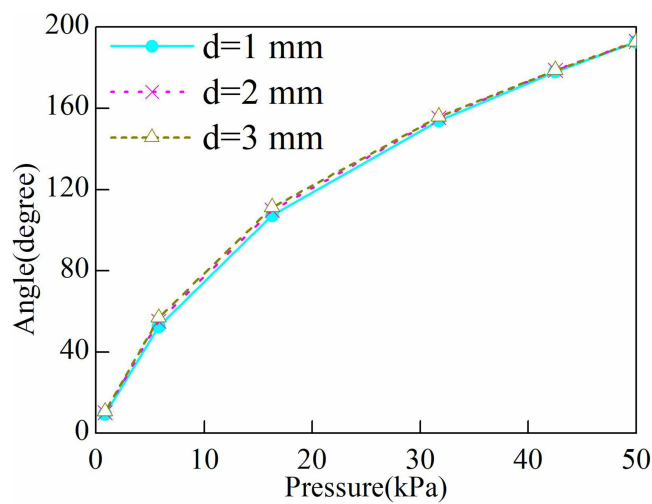**Figure 27** Influence of chamber width on end output force.

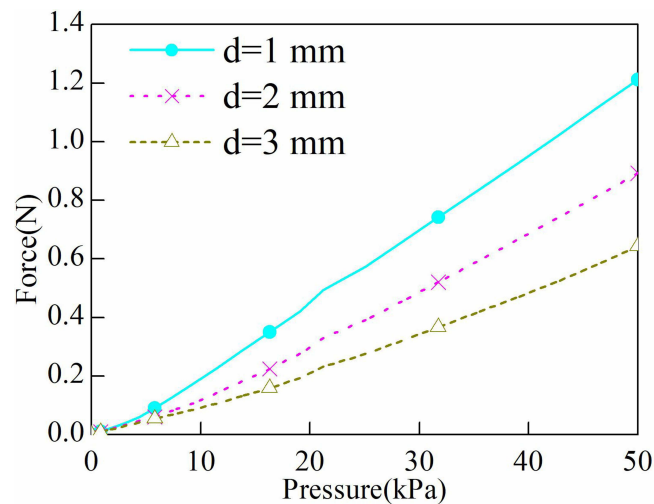**Figure 28** Influence of chamber spacing on bending angle.

Figure 29 Influence of chamber spacing on end output force.

air pressure, as the chamber spacing decreases, the terminal output force exhibits an increasing trend. This effect arises because, in the calculation of terminal output force, a displacement constraint in the Y direction is applied to the nodes at the bottom end. Under the applied air pressure, reducing the chamber spacing makes the inner walls of adjacent chambers more likely to contact and compress against each other. This intensified contact and compression cause the actuator to bend towards the constrained side at the bottom end, thereby increasing the terminal output force. To enhance the terminal output force while considering manufacturability, a spacing of d=1mm was ultimately chosen.

The Impact of Chamber Length

Chamber length L1 was set at 4.5 mm, 6 mm, and 7.5 mm for computational analysis, with the results for bending angle and terminal output force displayed in Figures 30 and 31, respectively. The figures show that chamber length has a notable impact on the bending angle of the actuator and a significant effect on the terminal output force. Under the same air pressure, as the chamber length increases, both the bending angle and the terminal output force exhibit a decreasing trend. To maximize the terminal output force while considering manufacturability, a chamber length of L1=4.5 mm was ultimately selected.
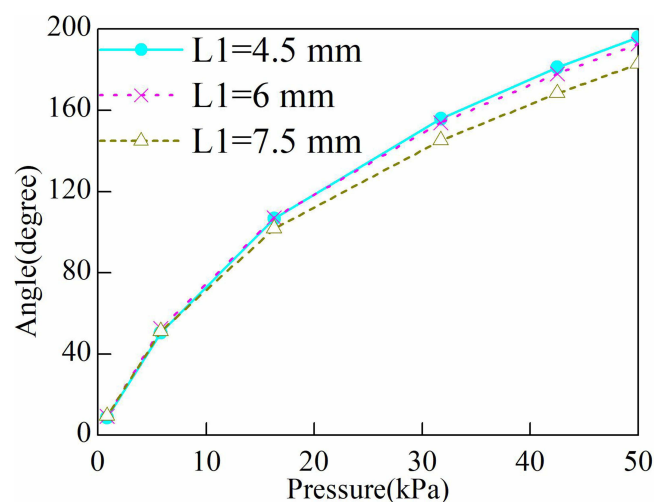

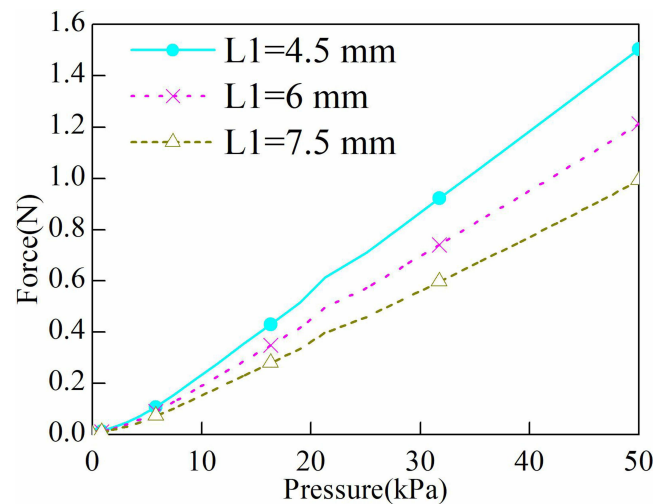**Figure 30** Influence of chamber length on bending angle.

Figure 31 Influence of chamber length on end output force.

The Impact of Chamber Number

Chamber count n was analyzed with values of 3, 4, and 5, with the results for bending angle and terminal output force displayed in Figures 32 and 33, respectively. The computational results indicate that the number of chambers significantly affects the performance of the actuator. Under the same air pressure, an increase in the number of chambers leads to an increase in the bending angle of the actuator, while the terminal output force shows a decreasing trend. A higher number of chambers results in a longer actuator, which can adversely affect the wearable comfort level. Based on the dimensional characteristics of the finger joints, both the MCP and PIP actuators have been designed with four chambers, while the DIP actuator has three chambers.

Comparative Analysis Before and After Structural Improvements

By establishing a finite element simulation model of the actuator, the influence of various parameters on the bending angle and output force of the actuator under different numerical values is analyzed. Then, considering the feasibility of manufacturing the actuator and the requirements for wearing comfort, the most reasonable values for each parameter are determined based on the regular curves in Sections 3.1–3.8, thus determining the final improvement plan. The sizes of various parameters before and after the structural improvement are shown in Table 2. Since the number of chambers for
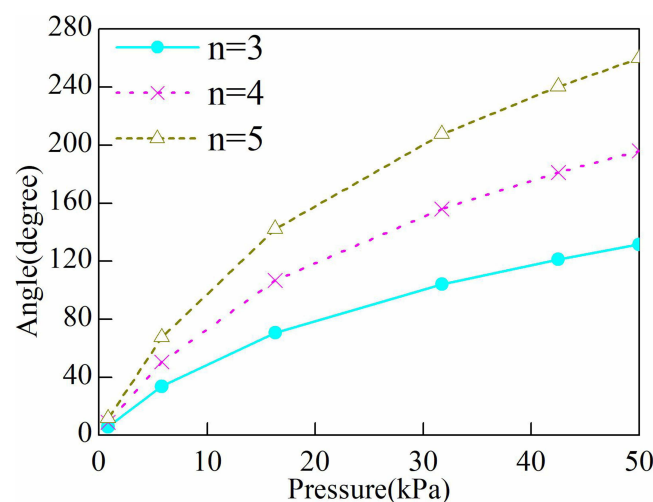

Figure 32 Influence of chamber quantity on bending angle.
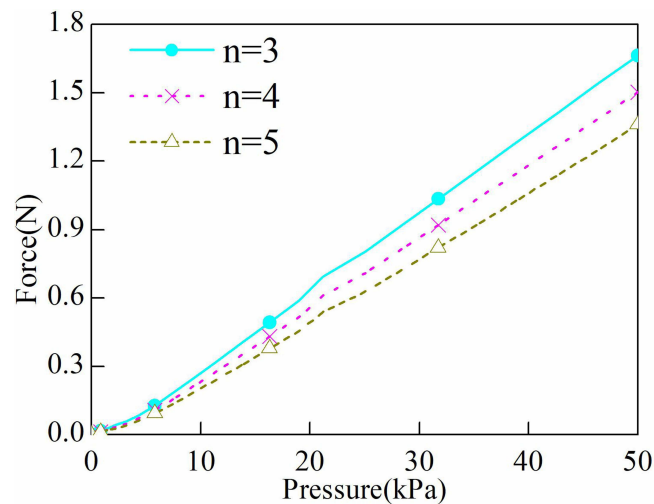
Figure 33 Influence of chamber quantity on end output force.

both the MCP driver and the PIP driver remains unchanged before and after the improvement (both are 4), for the sake of illustrating the significant improvement effect, a comparison of the bending angle and end output force before and after the improvement of the MCP driver is given here. Refer to Figures 34 and 35.

From Figure 34, it can be seen that when the input pressure is 50 kPa, the bending angle before improvement is 122.13°, and the bending angle after improvement is 196.08°, an increase of 60.6%. From Figure 35, it can be seen that the end output force before improvement is 0.61 N, and the end output force after improvement is 1.50 N, an increase of 145.9%. It can be seen that the performance of the joint actuator has been significantly improved after the improvement.

Analysis of Whole Finger Actuation Performance

Based on the improvement results of the parameters mentioned above, the structure of the soft actuator was redesigned. The dimensions of the improved soft actuator are shown in Figure 36. In Figure 36, A-A represents the overall cross-sectional view dimensions of the actuator, while B-B, C-C, and D-D represent the dimensions of the lateral cross-sectional views of the actuator at different positions, all measured in millimeters. A complete three-dimensional model of the soft actuator was established using CAXA software, as shown in Figure 37. Subsequently, finite element modeling was conducted.

During the use of the soft actuator, it is necessary to attach the actuator's joint sections to a rehabilitation glove. Therefore, when calculating the output force driven by individual joints, specific constraints need to be considered.

Table 2 Comparison of Structural Parameters Before and After Improvement

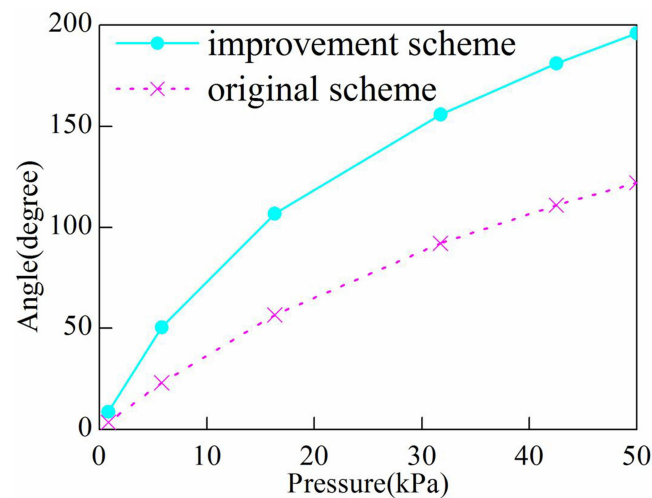| Parameters	Initial value	Modified value
t1(mm)	3	2
t2(mm)	2	1.5
t3(mm)	2	2
t4(mm)	2	2
t5(mm)	2	1.5
t6(mm)	2	2
h(mm)	10	12
b(mm)	16	16
d(mm)	2	1
L1(mm)	6	4.5

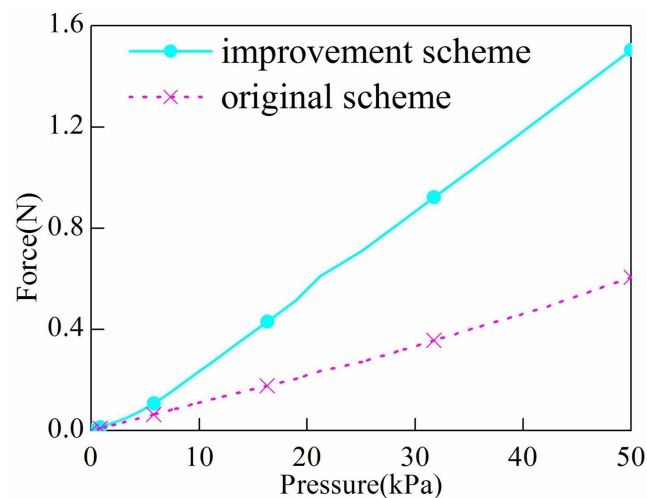**Figure 34** Comparison of Bending Angles Before and After Improvement.

Figure 35 Comparison of End Output Force Before and After Improvement.

Taking the calculation of the joint driving force when the PIP joint is driven independently as an example, a displacement constraint in the Y-direction is applied to the middle region of the PP, while displacement constraints in the Y-direction are also imposed on the nodes at the base of the MP. The output force of the actuator can then be equivalently determined by the reactive forces at these constrained nodes of the MP, as illustrated in Figure 38.

The results for whole finger bending deformation and output forces are shown in Figures 39 and 40 respectively. (Figure 39a) displays the displacement contour map of the MCP actuator when air pressure is independently input at 13.5 kPa, resulting in an MCP rotation of approximately 95°. (Figure 39b) shows the displacement contour map of the PIP actuator with an independent air pressure input of 13.5 kPa, resulting in a PIP rotation of about 94°. (Figure 39c) illustrates the displacement contour map of the DIP actuator when air pressure is independently input at 25 kPa, with a DIP rotation of approximately 90°. (Figure 39d) shows the displacement contour maps when air pressure is simultaneously applied to all joint actuators, with the MCP and PIP actuators at 13.5 kPa and the DIP actuator at 25 kPa. From Figure 39, it is evident that when air is separately inflated into the MCP, PIP, and DIP actuators, each joint can move independently under the influence of air pressure. The soft actuator bends only in the areas that align with the joints, while the sections that align with the knuckles do not bend. When air is simultaneously inflated into the MCP, PIP,
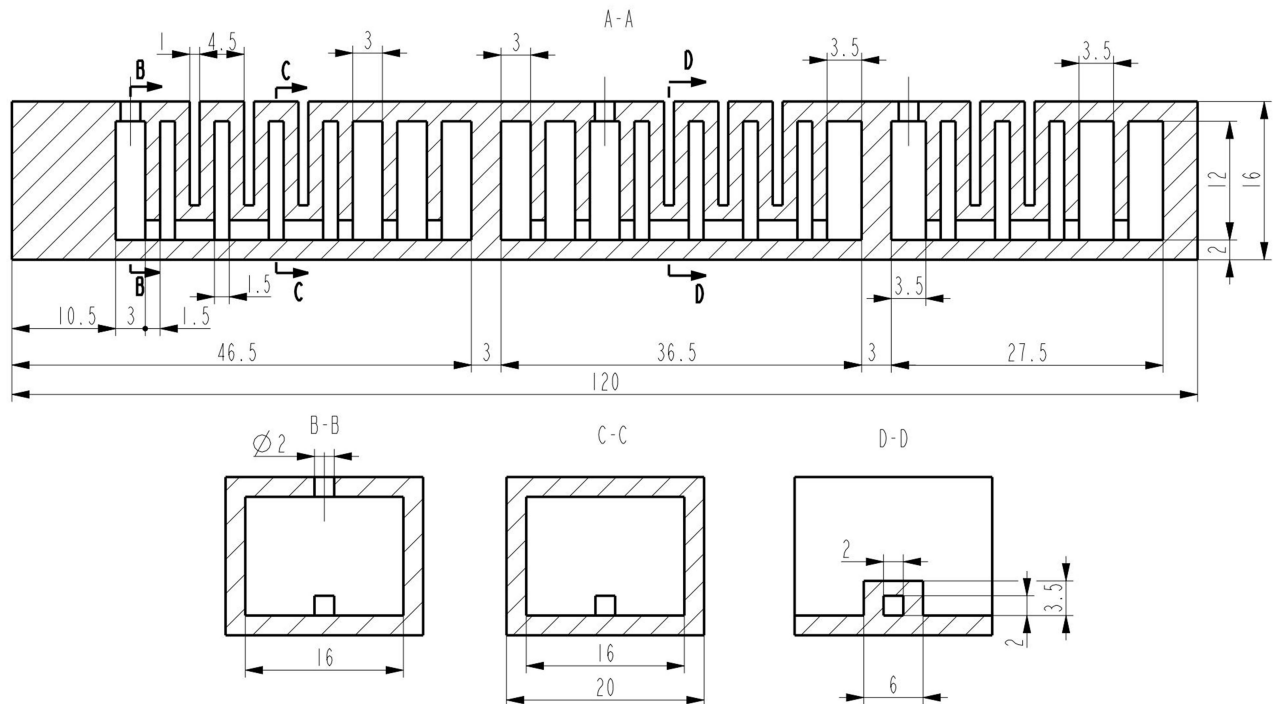
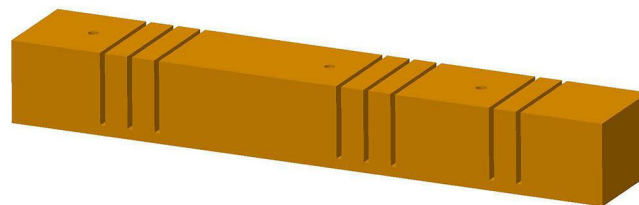**Figure 36** The dimension diagram of the improved soft actuator after enhancement.

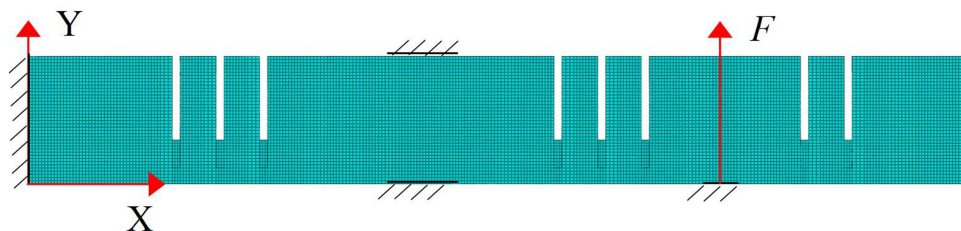**Figure 37** Modeling of the improved soft actuator.

Figure 38 Schematic diagram of force calculation when PIP is individually driven.

and DIP actuators, all three joints bend simultaneously, and the bending shape resembles the bending contour of a finger. Extracting the displacement of nodes along the axis direction at the bottom of the actuator, it can be obtained that the elongation of the bottom of the actuator is 7.8 mm when all three joints are pressurized to 50 kPa. This can compensate to some extent for the expansion of the skin in the joint area when the hand is bent, to better fit the hand.

From Figure 40, it is observed that when the input air pressure is set at 100 kPa, the output forces are as follows: the MCP actuator generates 3.22 N, the PIP actuator generates 3.06 N, and the DIP actuator produces 4.05 N. These values
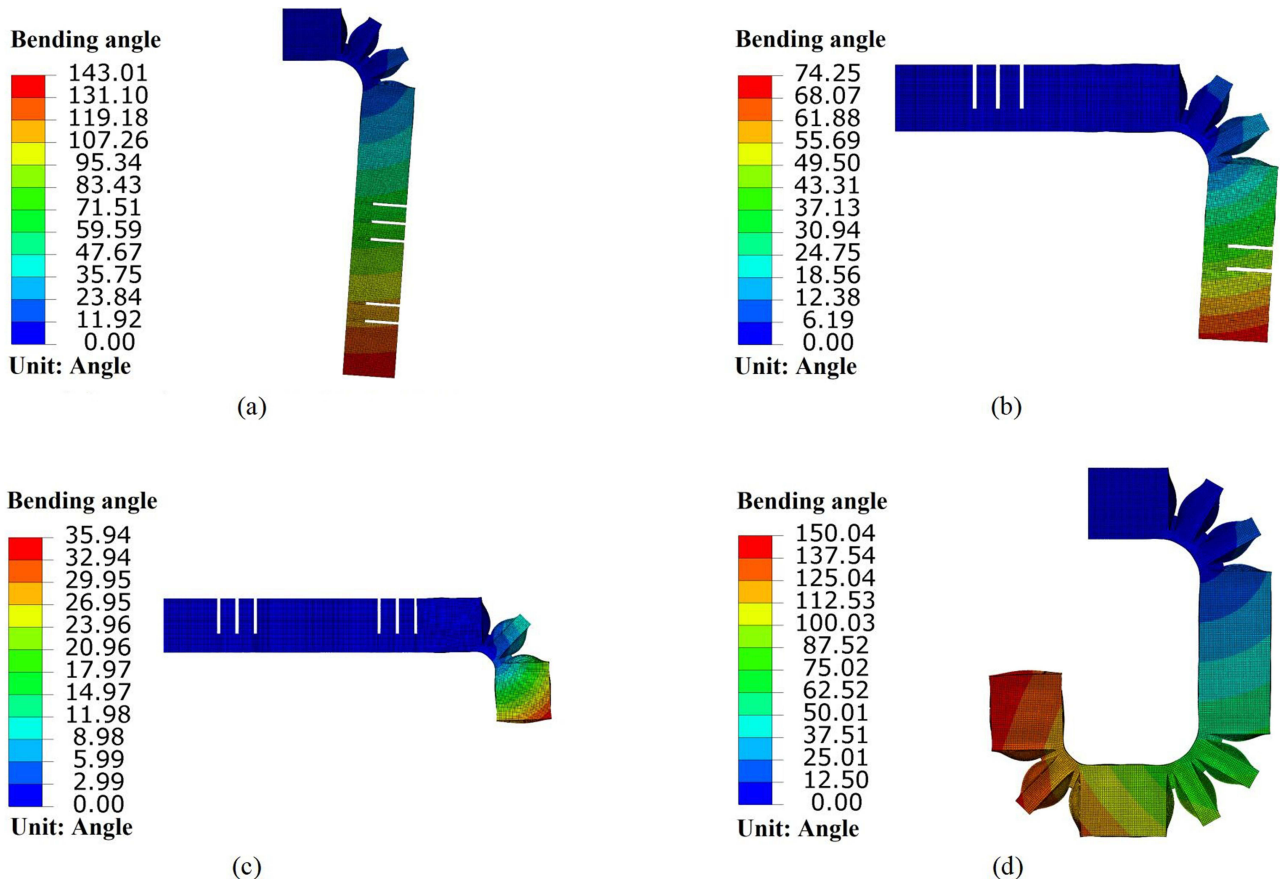
Figure 39 Displacement cloud map of the soft actuator. (**a**) displays the displacement contour map of the MCP actuator when air pressure is independently input at 13.5 kPa, resulting in an MCP rotation of approximately 95°. (**b**) shows the displacement contour map of the PIP actuator with an independent air pressure input of 13.5 kPa, resulting in a PIP rotation of about 94°. (**c**) illustrates the displacement contour map of the DIP actuator when air pressure is independently input at 25 kPa, with a DIP rotation of approximately 90°. (**d**) shows the displacement contour maps when air pressure is simultaneously applied to all joint actuators, with the MCP and PIP actuators at 13.5 kPa and the DIP actuator at 25 kPa.
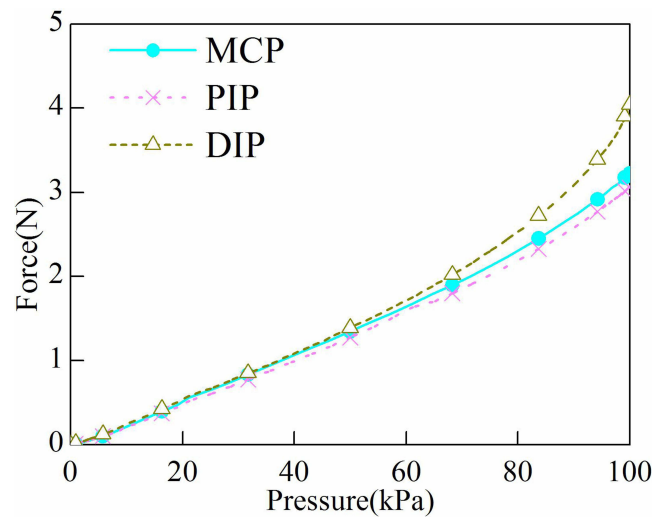

Figure 40 Results of force calculation when each joint is individually driven.

are all higher than the maximum joint output force of 2.15 N reported in Literature,[18] indicating that the actuator designed in this study meets the force requirements for finger rehabilitation training. Consequently, the designed soft actuator can fulfill the needs of finger rehabilitation training.

Conclusion

Considering the Human-machine ergonomics required for finger rehabilitation training, a segmented soft actuator was designed based on pneumatic network principles. The finger joint utilizes a fast pneumatic network structure, and the phalanx uses a slow pneumatic network structure, enhancing the fit between the soft actuator and the fingers. Each joint actuator is driven independently through its air channel, increasing the flexibility of the soft actuator's movements. The performance of the designed soft actuator was analyzed using the finite element method and compared with results from fPN and FBA analyses. The results show that under the same air pressure, the actuator designed in this study offers superior driving performance. The impact of structural dimensional parameters on the bending characteristics and terminal output force of the actuator was analyzed, indicating that the thickness of the constraining layer, inner wall thickness of the chamber, chamber height, chamber width, chamber spacing, chamber length, and the number of chambers have a very significant effect on the actuator's performance. Based on these findings, optimal structural parameters were obtained, effectively enhancing the actuator's performance. Numerical analysis of the whole finger bending process showed that under independent or coupled joint movements, the soft actuator's bending angle, bending shape, and joint driving force all meet the requirements for finger rehabilitation training. This research provides a reference for the design of soft actuators and offers reliable theoretical support for their application in hand assistance and rehabilitation.

Data Sharing Statement

The data that support the findings of this study are available from the corresponding author upon reasonable request.

Acknowledgments

Disclosure

The authors declare that they have no conflicts of interest in this work.

References

1. Li G, Cheng L, Gao Z, et al. Development of an untethered adaptive thumb exoskeleton for delicate rehabilitation assistance. *IEEE Trans Rob*. 2022;38(6):3514–3529. doi:10.1109/TRO.2022.3180832
2. Tian Y, Wang H, Liu Y, et al. Design and analysis of an exoskeleton robot for index finger rehabilitation. *J Mech Eng*. 2023;59(09):40–50.
3. Bützer T, Lambercy O, Arata J, et al. Fully wearable actuated soft exoskeleton for grasping assistance in everyday activities. *Soft Rob*. 2021;8 (2):128–143. doi:10.1089/soro.2019.0135
4. Li G, Cheng L, Zhang C. Design and modeling of a bioinspired flexible finger exoskeleton for strength augmentation. IEEE/ASME Transactions on Mechatronics; 2024.
5. Hu W, Alici G. Bioinspired three-dimensional -printed helical soft pneumatic actuators and their characterization. *Soft Rob*. 2020;7(3):267–282. doi:10.1089/soro.2019.0015
6. Li H, Yao J, Zhou P, et al. High-force soft pneumatic actuators based on novel casting method for robotic applications. *Sens Actuat A Phys*. 2020;306:111957. doi:10.1016/j.sna.2020.111957
7. Manti M, Hassan T, Passetti G, et al. A bioinspired soft robotic gripper for adaptable and effective grasping. *Soft Rob*. 2015;2(3):107–116. doi:10.1089/soro.2015.0009
8. Duduta M, Berlinger F, Nagpal R, et al. Tunable multi-modal locomotion in soft dielectric elastomer robots. *IEEE Rob Autom Lett*. 2020;5 (3):3868–3875. doi:10.1109/LRA.2020.2983705
9. Liu M, Hao L, Zhang W, et al. A novel design of shape-memory alloy-based soft robotic gripper with variable stiffness. *Int J Adv Rob Syst*. 2020;17 (1):1729881420907813. doi:10.1177/1729881420907813
10. Mosadegh B, Polygerinos P, Keplinger C, et al. Pneumatic networks for soft robotics that actuate rapidly. *Adv Funct Mater*. 2014;24 (15):2163–2170. doi:10.1002/adfm.201303288
11. Polygerinos P, Lyne S, Wang Z, et al. Towards a soft pneumatic glove for hand rehabilitation[C]//2013 IEEE/RSJ International Conference on Intelligent Robots and Systems. IEEE; 2013: 1512–1517.

12. Li K, Bi X, Li L, et al. Wearable robot for hand rehabilitation based on a pneumatic soft actuator. *Machine Tool Hydraulics*. 2022;50(23):30–34.
13. Cappello L, Meyer JT, Galloway KC, et al. Assisting hand function after spinal cord injury with a fabric-based soft robotic glove. *J Neuroeng Rehabil*. 2018;15:1–10. doi:10.1186/s12984-018-0391-x
14. Polygerinos P, Wang Z, Galloway KC, et al. Soft robotic glove for combined assistance and at-home rehabilitation. *Rob Auton Syst*. 2015;73:135–143. doi:10.1016/j.robot.2014.08.014
15. Li X, Hao Y, Zhang J, et al. Design, modeling and experiments of a variable stiffness soft robotic glove for stroke patients with clenched fist deformity. IEEE Robotics and Automation Letters, 2023.
16. Wang J, Fei Y, Pang W. Design, modeling, and testing of a soft pneumatic glove with segmented prevents bending actuators. *IEEE ASME Trans Mechatron*. 2019;24(3):990–1001. doi:10.1109/TMECH.2019.2911992
17. Wang F, Chen Y, Wang Y, et al. A soft pneumatic glove with multiple rehabilitation postures and assisted grasping modes. *Sens Actuat A Phys*. 2022;347:113978. doi:10.1016/j.sna.2022.113978
18. Liu CX, Pan TT, Sun YF, et al. Segmented pneumatic soft actuator for rehabilitation training. *J Zhejiang Univ*. 2022;56(06):1127–1134.
19. Sun K, Tian Y. Numerical investigation of a bioinspired multi-segment soft pneumatic actuator for grasping applications. *Mater Today Commun*. 2022;31:103449. doi:10.1016/j.mtcomm.2022.103449
20. Gariya N, Kumar P, Prasad B Stress and bending analysis of a soft pneumatic actuator considering different hyperelastic materials. Materials Today: Proceedings, 2022, 65: 3126–3131.
21. Yang WT, Stuart HS, Tomizuka M. Mechanical modeling and optimal model-based design of a soft pneumatic actuator[C]//2023. IEEE International Conference on Soft Robotics (RoboSoft). IEEE; 2023: 1–7.
22. Liao Z, Li T, Wang Y, et al. Soft pneumatic actuator optimal design based on isogeometric analysis. *Manuf Lett*. 2023;35:55–63. doi:10.1016/j.mfglet.2023.08.001
23. Hu W, Mutlu R, Li W, et al. A structural optimization method for a soft pneumatic actuator. *robotics*. 2018;7(2):24. doi:10.3390/robotics7020024
24. Yang F, Ruan Q, Man Y, et al. Design and optimize of a novel segmented soft pneumatic actuator. *IEEE Access*. 2020;8:122304–122313. doi:10.1109/ACCESS.2020.3006865
25. Lee SI, Song EJ, Yun YI, et al. Soft pneumatic actuator workspace augmentation with synthesis of simplified analytical and numerical subcomponent models. *Sens Actuat A Phys*. 2024;365:114814. doi:10.1016/j.sna.2023.114814
26. Hong D. *Human Kinematics*. Beijing: People's Health Publishing House; 2008:103–115.
27. Zhang Z, Calderon AD, Huang X, Huang A. Research status and prospect of finger rehabilitation machinery. *Med Devices*. 2024;17:1–22. doi:10.2147/MDER.S429206
28. Qinchao Z. *Design and Research of the Mechanical System for a Hand Rehabilitation Robot*. Harbin Institute of Technology; 2012.